Polymer 49 (2008) 3611–3618

Contents lists available at ScienceDirect

Polymer

journal homepage: www.elsevier.com/locate/polymer

Feature Article

Excess free energy of nanoparticles in a polymer brush

A. Milchev [a,b,*], D.I. Dimitrov [a], K. Binder [a]

[a] Institut für Physik, Johannes Gutenberg Universität Mainz, Staudinger Weg 7, 55099 Mainz, Germany
[b] Institute for Chemical Physics, Bulgarian Academy of Sciences, 1113 Sofia, Bulgaria

ARTICLE INFO

Article history:
Received 25 January 2008
Received in revised form 7 April 2008
Accepted 17 April 2008
Available online 25 April 2008

Keywords:
Nanoinclusions
Nanocolloids
Polymer brush
Monte Carlo
Free energy

ABSTRACT

We present an efficient method for direct determination of the excess free energy ΔF of a nanoparticle inserted into a polymer brush. In contrast to Widom's insertion method, the present approach can be efficiently implemented by Monte Carlo or Molecular Dynamics methods also in a dense environment. In the present investigation the method is used to determine the free energy penalty $\Delta F(R, D)$ for placing a spherical particle with an arbitrary radius R at different positions D between the grafting plane and the brush surface. Deep inside the brush, or for dense brushes, one finds $\Delta F \propto R^3$ whereas for shallow nanoclusions $\Delta F \propto R^2$, regardless of the particle interaction (attractive/repulsive) with the polymer.
The pressure and density fields around spherical nanoinclusions in a polymer brush are also investigated. Extensive Monte Carlo simulations show that the force, exerted on the particle by the surrounding brush, depends essentially on the proximity of the nanocolloid particle to the brush surface not only in strength but also with respect to its angular distribution. For shallow nanoinclusions close to the brush surface this angular distribution is shown to result in a growing buoyant force while deep inside the brush this effect is negligible.

1. Introduction

Spatially extended arrangements of nanoparticles embedded in various polymer materials have found much interest in the development of novel materials [1–19]. Already very small volume fractions of nanoparticles suffice to significantly modify properties such as permeability, etc. Nanostructured polymeric materials containing nanoparticles can be considered as "designer materials" [9] that hold great promise for tailoring material properties. "Smart" micro-gel particles [19] may find important application in catalysis, biolabeling, chemical and biological separations.

Particularly interesting polymer films with nanoinclusions are provided by polymer brushes [9,18], since already without nanoparticles being present polymer brushes have an interesting self-organized structure, with spatial inhomogeneity in direction perpendicular to the grafting surface [20–25]. It has been predicted [9,18] that the interaction of the nanoparticles with the polymers in such a polymer brush may lead to very interesting pattern formation. However, the current theoretical understanding of the nanoparticle pattern formation in polymer brushes is based on rather simplified models, and a more detailed investigation of the nanoparticle–brush interaction is desirable.

A central problem in understanding the behavior of nanoinclusions in a polymer brush is the computation of their excess free energy ΔF which, as with all entropy related quantities, is usually not straightforward in a simulation. The knowledge of ΔF and its variation with the size of the nanoinclusion or the position inside the polymer brush is crucial for the determination of the penetration depth of such particles into polymer coatings, their concentration profiles, and even for possible phase transitions the nanoinclusions might undergo upon changing the relevant parameters of the system. A standard approach for the calculation of ΔF, is Widom's test particle insertion method [26], however, the method becomes rapidly less practicable as the density of the system increases. The present paper tries to take a first step to fill this gap by presenting a simulation study of a single nanoparticle embedded in a polymer brush. Our work is based on a coarse-grained off-lattice model of flexible polymer chains [27–31] which has been very useful for the description of both dilute, semidilute and concentrated polymer solutions [27,30], adsorbed polymer films at a surface [29], and polymer melt droplets [31]. This model is very well suited to study polymer brushes, and in Section 2 we briefly describe its main properties and our procedures to equilibrate such brushes when a single nanoparticle is inserted. Section 3 then gives results for the energy of the nanoparticle and the 'buoyant force' it experiences for a range of values of its radius R and the height D at which its center of mass is located above the grafting surface. Also the distortion of the bulk structure near the nanoparticle is analyzed, and the anisotropic character of the forces

* Corresponding author. Institut für Physik, Johannes Gutenberg Universität Mainz, Staudinger Weg 7, 55099 Mainz, Germany.
E-mail address: milchev@ipc.bas.bg (A. Milchev).

0032-3861/$ – see front matter © 2008 Published by Elsevier Ltd.
doi:10.1016/j.polymer.2008.04.032

acting on it is discussed. The method for calculation of the excess free energy is presented and validated in Section 4 along with some first findings about the properties of $\Delta F(R, D)$. Section 5 then provides a brief discussion of the results and points out the difficulties that still need to be overcome if one wishes to simulate a system containing many nanoparticles.

2. Model

We have used a coarse-grained off-lattice bead spring model [27,28] to describe the polymer chains in our system. The polymer brush consists of linear chains of length N grafted at one end to a flat structureless surface. The effective bonded interaction is described by the FENE (finitely extensible nonlinear elastic) potential,

$$U_{\mathrm{FENE}} = -K(l_{\max} - l_0)^2 \ln\left[1 - \left(\frac{l - l_0}{l_{\max} - l_0}\right)^2\right] \quad (1)$$

with $K = 20$, $l_{\max} = 1$, $l_0 = 0.7$, $l_{\min} = 0.4$ – Fig. 1. Thus the equilibrium bond length between the nearest neighbor monomers is $l_0 = 0.7$. Here and in what follows we use the maximal extension of the bonds, $l_{\max} = 1$, as our unit length while the potential strength is measured in units of thermal energy k_BT where k_B is the Boltzmann constant.

The nonbonded interactions are described by the Morse potential,

$$\frac{U_M(r)}{\epsilon_M} = \exp(-2\alpha(r - r_{\min})) - 2\exp(-\alpha(r - r_{\min})), \quad (2)$$

with $\alpha = 24$, $r_{\min} = 0.8$, $\epsilon_M/k_BT = 1$.

The polymer chains are tethered to grafting sites which constitute a triangular periodic lattice on the substrate whereby the closest distance between the grafting sites is l_0. Thus the largest grafting density $\Sigma = 1.0$, if the polymer chains are anchored at distance l_0, and $\Sigma = 0.25$, if the 'lattice constant', i.e., the distance between adjacent head monomers on the surface is equal to $2l_0$. In most of our simulation studies we have investigated dense brushes $\Sigma = 1.0$ as being the most demanding ones, however, also some studies of grafting density $\Sigma = 0.25$ have been performed. Note that $\Sigma = 1.0$ corresponds to a simulation where the monomer density in the brush near the wall is close to the density of a polymer melt while $\Sigma = 0.25$ would correspond to a rather concentrated polymer solution.

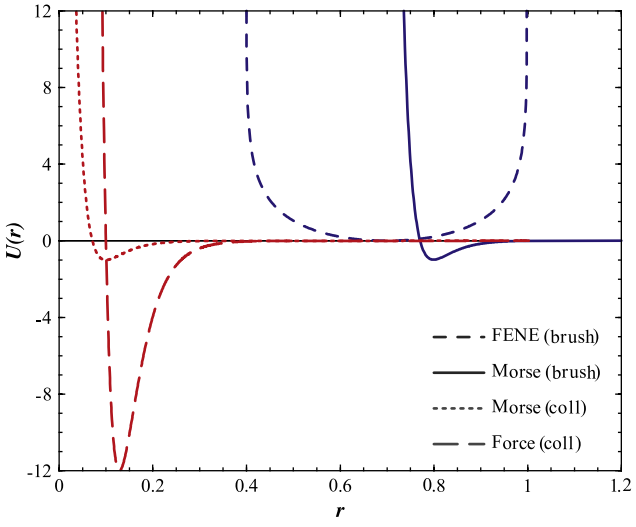

Fig. 1. Plot of the interactions used in the present study.

For the chain model, $\epsilon_M/k_BT = 1$ corresponds to good solvent conditions since the Theta-point for a (dilute) solution of polymers described by the model, Eqs. (1) and (2), has been estimated [27] as $k_B\Theta/\epsilon_M = 0.62$. In all our simulations we use brushes formed by polymer chains consisting of N effective monomers whereby $16 \le N \le 64$. Note that, as usual, solvent molecules are not explicitly included [28–30] but work which includes solvent explicitly [25] would yield very similar results.

The nanoinclusion is taken as a spherical (nanocolloid) particle of radius R at distance D away from the grafting surface. We consider both attractive and repulsive interactions of the nanocolloid with the monomers of the brush and the colloid potential is again modeled as a Morse potential, Eq. (2), 'smeared' at the surface of the spherical particle, with a much shorter range, $r_{\min}^{\mathrm{coll}} = 0.1$ – cf. Fig. 1. Using Eq. (2) for the interaction between a monomer and the colloidal particle, it is hence understood that r is the normal distance between the monomer and the spherical surface (the latter itself being at distance R from the center of mass of the colloidal particle). Thus $r_{\min}^{\mathrm{coll}}$ in Eq. (2) is replaced by r_c while α and ϵ_M are taken to be the same as for the monomer–monomer interaction. Since the radius of the spherical particle has been varied in a rather broad interval, $0.05 \le R \le 3.0$, exceeding considerably that of the monomers, $l_0/2 = 0.35$, a special care has been taken to prepare well equilibrated initial configurations of the polymer brush with inclusion. To this end two different methods, "particle indentation", and "particle inflation" were employed.

We found out that the indentation method, whereby the sphere of desired radius R is inserted through the surface into the brush by small vertical displacements of sphere's center, does not provide satisfactory results. For dense polymer brushes this indentation method strongly deforms the chains underneath the sphere. These resulting distortions in the brush structure could not subsequently relax to equilibrium conformations within the time scale of the simulation experiment. In the *particle inflation* method a spherical particle of vanishing radius is originally placed at distance $D = D' + R$ from the grafting plane (here and below D' denotes the closest distance between the particle surface and the grafting plane) whereupon the polymer environment around it is equilibrated. Then the particle radius is increased, $R \to R + \Delta R$, by a small margin $\Delta R = 0.05$ and the system is equilibrated again. This equilibration takes typically about 10% of the time in Monte Carlo steps (MCS) per monomer, needed for the subsequent measurement runs. A series of such steps quickly creates well equilibrated conformations of the polymer brush around an inclusion for arbitrary distances D and radii R. Thus we study the phenomena for a wide range of choices for R by preparing initial configurations for any given distance D. Once such initial configurations are available, measurements of relevant characteristic parameters of the system can be readily carried out.

For a dense brush with polymer chains of lengths $N = 16$, 32, statistical averages were derived from typically 1.6×10^7 Monte Carlo steps (MCS) per monomer. The Monte Carlo algorithm consists of attempted moves whereby a monomer is chosen at random and one attempts to displace it to a new randomly chosen position $-0.5 \le \Delta x, \Delta y, \Delta z \le 0.5$ regarding the old position. We use periodic boundary conditions in the x, y directions and impenetrable walls in the z direction. Two typical configurations of the polymer brush with a spherical inclusion are shown in Fig. 2. In Fig. 2a we display a "shallow" inclusion, and in Fig. 2b – a "deep" one. As we shall see in the following, shallow and deep nanoinclusions differ essentially in their properties. In the course of the simulations we also sample the concentration profile of the monomers around the spherical particle as well as its internal energy, the buoyant force, exerted by the brush perpendicular to the grafting surface as well as the angular distribution of the total force, acting on the nanocolloid particle, in terms of the polar angle θ with the z-axis.

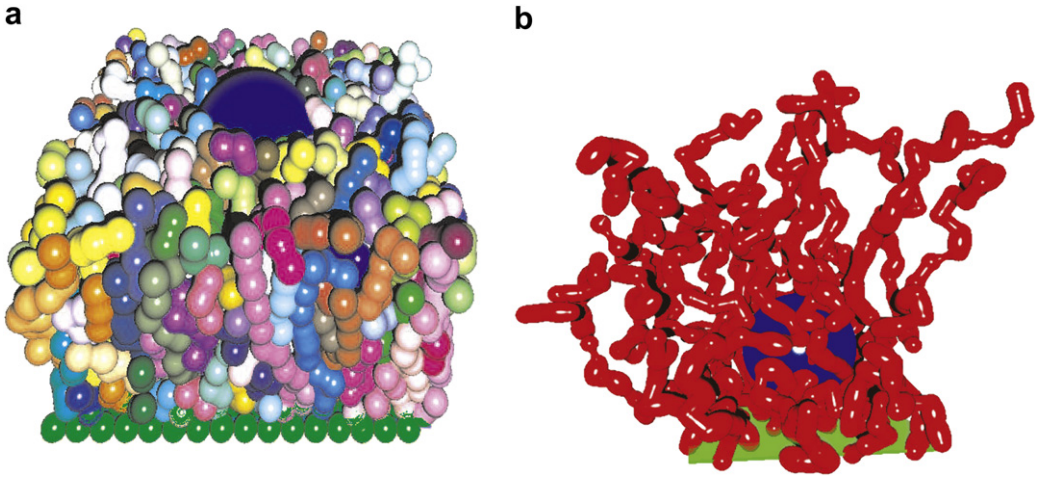

Fig. 2. Snapshot of a nanocolloid particle in a polymer brush: (a) $R = 3.0$, $D = 10.0$, $N = 16$, $\Sigma = 1.0$, (b) $R = 2.1$, $D = 5.1$, $N = 32$, $\Sigma = 0.25$.

3. Results

In Fig. 3 we show several typical profiles of the total monomer density distribution in the direction perpendicular to the grafting plane of a polymer brush. For dense brushes, $\Sigma = 1.0$, one observes the characteristic layering of the monomers in the vicinity if the wall which vanishes after 4–5 molecular distances. Similar albeit more weakly expressed layering is also observed around the spherical nanoinclusion itself. Evidently, in the loose brush, $\Sigma = 0.25$, these effects of steric repulsion and layering are absent. Instead, one finds an area of depleted monomer density at immediate vicinity of the particle's surface. The density profile of chain ends $\rho(z)$ (which is displayed normalized to unity for better comparison with $\phi(z)$) demonstrates that chain ends are distributed not merely on the surface but throughout the polymer brush. These profiles are very similar to those obtained from previous simulations of other coarse-grained models for dense polymer brushes [22,23]. The profile for $N = 32$, $\Sigma = 1.0$ is nearly constant for $3.0 \leq z \leq 12.0$ while at $z \approx 14.0$ its faster decrease manifests the proximity of the brush surface. One may expect, therefore, that typical quantities pertaining to the spherical inclusion like the local brush deformation around it, or the resulting force which acts on the particle, will change little as far as $D + R$ is sufficiently far below the top of this polymer brush. For larger or shallower inclusions, however, one would expect marked changes in these properties for $D + R \geq 13.0$.

The impact of a large spherical inclusion on the surrounding polymer brush is shown in Fig. 4 where only the left part of the monomer concentration in the area between the center of the nanocolloid and the grafting walls is displayed. For the semidilute brush with $\Sigma = 0.25$, Fig. 4a, one can see a depletion region around the particle which extends several molecular diameters away from the nanocolloid surface and then smoothly goes over to the unperturbed concentration profile of the polymer brush. The sphere at $D = 10.0$ is located in the tail of the loose brush – cf. Fig. 3 – so that the nanocolloid is half immersed in the brush. Some minor distortion of the monomer density profile is indicated by the isodensity contour lines close to the right edge of the graph. In contrast, for $\Sigma = 1.0$ the density perturbation around the sphere is much larger and several concentric density oscillations around the nanocolloid surface indicate typical layering effects – Fig. 4b. Since the dense brush stretches much further, at the same position $D = 10.0$ the nanocolloid is placed deep inside the brush, and the density undulations around it are symmetric. In Fig. 5 we examine the variation of the internal energy U and the buoyant force f, exerted by the brush on a spherical particle at a distance D from the

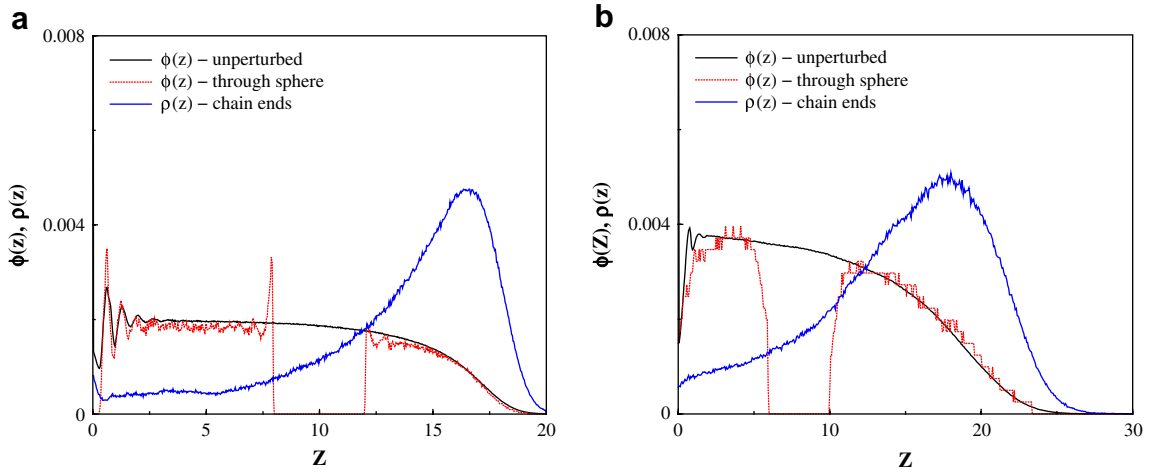

Fig. 3. Monomer density $\phi(z)$ at distance z from the grafting plane: no inclusion (full line) and across the inclusion (dotted line). The density distribution of chain ends $\rho(z)$ is also displayed. Shown are monomer density profiles with repulsive colloid-brush interaction: (a) $\Sigma = 1.0$, $N = 32$, $R = 2.0$, and $D = 10.0$, and (b) $\Sigma = 0.25$, $N = 64$, $R = 2.0$, and $D = 8.0$. The unperturbed monomer – $\phi(z)$ and chain ends density profiles $\rho(z)$ are normalized to unity for better visibility. The perturbed $\phi(z)$ is adjusted to match the unperturbed $\phi(z)$ far away from the nanocolloid particle.

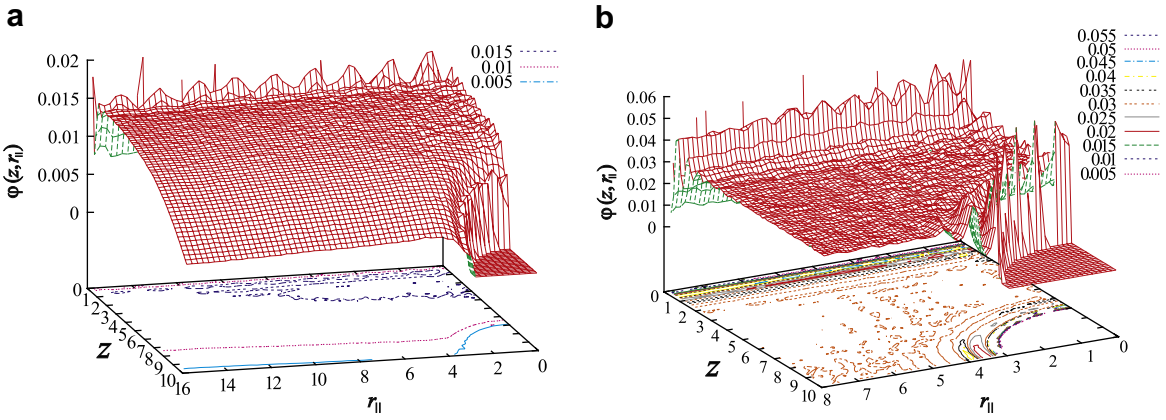

Fig. 4. Monomer density distribution in the vicinity of a nanocolloid particle for a polymer brush with chain length $N = 32$. The spherical particle with $R = 3$ is placed at distance $D = 10.0$ from the grafting plane. The density profile spans the area from the center of the particle (at the front right corner) up to the intersection of the container wall with the grafting plane along the z-axis. (a) Grafting density $\Sigma = 0.25$, and (b) $\Sigma = 1.0$.

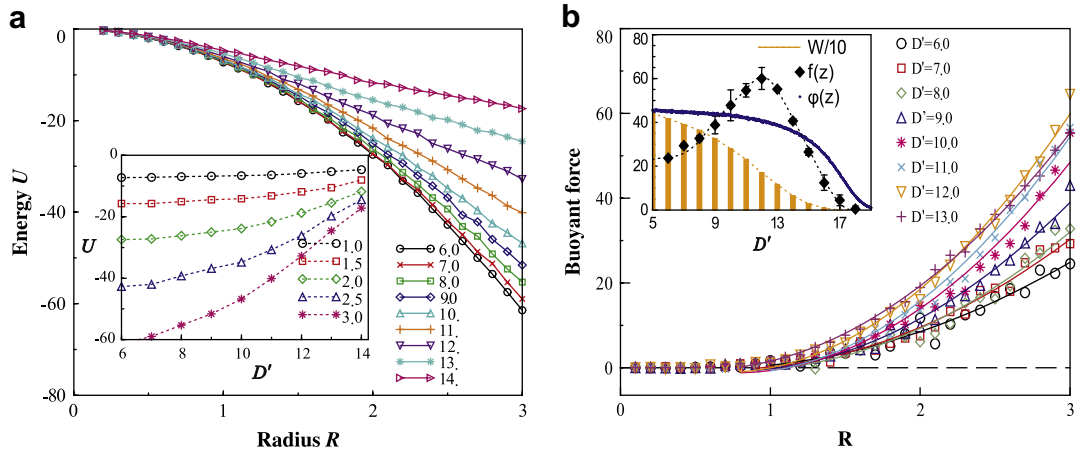

Fig. 5. (a) Energy U of a spherical particle against particle radius R at different distances $D' = D - R$ (given as a parameter) of the sphere surface from the grafting plane. Here $\Sigma = 1.0$ and $N = 32$. In the inset the variation of U with distance D' is plotted for several radii R (R is given as a parameter). (b) Buoyant force f exerted on the same particle by the polymer brush. Full lines denote a best fit with a 2nd-order polynomial. The inset shows $f(R = 3.0)$ for different distances D' from the grafting plane. The course of the monomer density profile is also given (appropriately normalized for better visibility). Vertical bars denote the work W (reduced for visibility by a factor of 10), which is necessary in order to place this nanoinclusion at depth D' between the sphere surface and the grafting plane.

grafting plane, against changing particle radius R. The force is computed from the derivative of the nanoparticle potential Eq. (2) with $r = r_{\min}^{\text{coll}}$ at the positions of the surrounding monomers. In Fig. 5b we plot only the component of f which is normal to the grafting plane (the buoyant force). In the particular case of Fig. 5 the interaction between brush monomers and inclusion is attractive and, as that between monomers, has the strength of k_BT, albeit the results with repulsive interactions between the particle and the monomers of the brush are qualitatively very similar. An inspection of Fig. 5a indicates one principal result of this study, namely, that the energy U increases (in absolute units) with the increase of R following a parabolic relationship, $U(R) \propto -R^2$, as long as the spherical inclusion stays deep inside the polymer brush $6.0 \le D' \le 11.0$. For shallow inclusions, $D' \ge 12.0$, the density field above the sphere is weaker and, therefore, not balanced by the field beneath whereby $U(R)$ deviates from parabolic shape for large enough R. The variation of U with distance D' away from the substrate reveals a similar relationship – see the inset in Fig. 5a. The absolute value of U gradually decreases as the sphere is moved towards the surface of the polymer brush, however, this effect fades out as the radius R becomes smaller.

Fig. 5b demonstrates (despite some scatter in our data) that the buoyant force, acting on the inclusion, increases with growing radius R in a parabolic way. It becomes clear from the inset in Fig. 5b that this force goes over from initially moderate into steeper increase for distances D' which fall into the faster diminishing part of the brush density profile. Thus f goes through a maximum and subsequently declines when the sphere radius R becomes so large that the density distortion around the nanocolloid reaches the brush surface so that the polymers do not surround tightly the inclusion. From the f versus D' relationship one may easily compute the work W, that is, $W = \int_{D'}^{\infty} f(z)\mathrm{d}z$, which has to be performed in order to place the spherical particle in position D inside the polymer brush. As demonstrated in the inset of Fig. 5b, for a big particle $R = 3.0$ this work grows steeply (for the sake of better visibility, W is reduced there by a factor of 10) as D' becomes smaller. Eventually we point out at this place that due to symmetry the lateral component of the total force, acting on the particle is always equal to zero.

Eventually, in Fig. 6 we show the angular distribution of the force, exerted on a nanocolloid particle of radius $R = 3.0$ for different depths of the nanocolloid inside a polymer brush. The polar angle $\theta = 0$ corresponds to a force directed along the positive z-axis. From Fig. 6 one may conclude that inclusions deep inside the polymer brush as, e.g. at $D' = 7.0$, experience predominantly symmetric forces which act laterally on them, and in result, cancel. As the inclusion comes closer to the brush surface, however, the forces acting on it redistribute angularly due to changes in the density

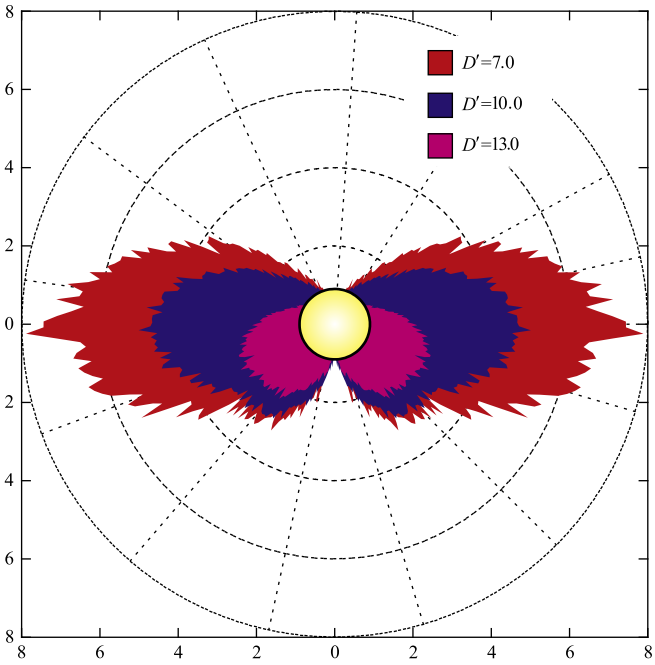

Fig. 6. Angular distribution of the force, exerted on a nanocolloid particle of radius $R = 3.0$ for different depths of the nanocolloid inside a polymer brush. The polar angle $0 \le \theta \le \pi$ is measured from the normal to the grafting plane which is placed at distance $D' = 7.0$ (red), 10.0 (blue) and 13.0 (purple) beneath the nanocolloid particle (green). The chain length is $N = 32$ and the grafting density $\Sigma = 1.0$. As the colloid approaches the upper end of the brush, the force decreases and redistributes from predominantly lateral into upward direction.

field around the particle – $D' = 13.0$ – and decline. Thus close beneath the brush surface there forms a resulting force which tends to expel the inclusion out of the polymer brush.

These findings are supported by the results shown in Fig. 7 too. In this figure we display the angular distribution of the force, exerted on a shallow inclusion at fixed distance $D' = 14.0$ slightly under the brush surface. Evidently, the smaller inclusion, $R = 1.0$, does not distort the density homogeneity of the surrounding polymer matrix, and the force field around it is distributed laterally and symmetrically as regards the z-axis. The large inclusion, $R = 3.0$, in contrast, induces a long range distortion field in its neighborhood, the brush partially opens above it, and a vertical component of the force, driving the inclusion out of the polymer matrix, emerges.

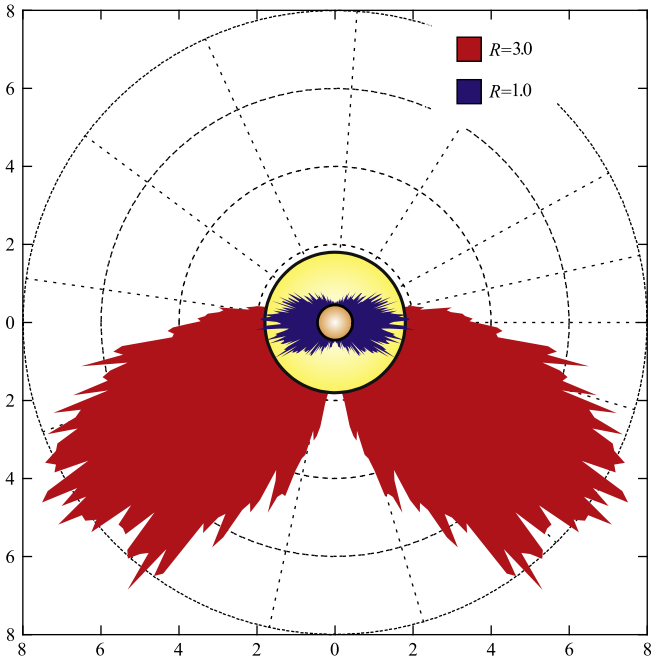

Fig. 7. The same as in Fig. 6 but for nanocolloids of different sizes, $R = 1.0$ and $R = 3.0$, close ($D = 14.0$) to the polymer brush surface. Although at the same position, the brush distortion by the smaller particle does not reach the brush end and, hence, the force is laterally distributed. The distortion field around the bigger nanocolloid reaches the free space above the brush end and the resultant force exerted by the brush acts upwards.

4. Free energy

As a rule, the computation of free energy differences ΔF relies on variants of *thermodynamic integration* (TI) or *thermodynamic perturbation* (TP) methods. In the present investigation we employ a TP procedure which is based on the identity [32–34],

$$\Delta F = -\beta^{-1} \ln\langle \exp(-\beta \Delta H)\rangle_\lambda, \quad (\Delta H \equiv H_\lambda - H_0) \tag{3}$$

where H is the Hamiltonian of the system, $\beta^{-1} = k_B T$, and $\langle\ \rangle_\lambda$ denotes a canonical average with respect to a fixed value of some parameter λ – in the present study this is the particle radius R. Using a method such as Monte Carlo, one essentially samples points in the phase space from a canonical distribution corresponding to $\lambda = 0$ and then takes the average of $\exp(-\beta\Delta H)$ over these points. In principle, the method should be exact, provided the number of sampled points tends to infinity. In practice, unless the canonical distributions, corresponding to H_0 and H_λ overlap to a significant degree, the average of the $\exp(-\beta\Delta H)$ will be dominated by points in phase space that are visited extremely rarely during the canonical sampling [35] which would impede the convergence as the sampling proceeds. In order to get around this problem we break the interval $0 \le \lambda \le R$ into small subintervals, $\Delta R \ll R$, and compute the free energy difference corresponding to each subinterval:

$$F(R + \Delta R) - F(R) = -\beta^{-1} \ln\left\langle e^{-\beta[U(R+\Delta R) - U(R)]}\right\rangle_{\Delta R}. \tag{4}$$

In Eq. (4) $U(R)$ denotes the internal energy of a nanocolloid particle of radius R, embedded in a well equilibrated polymer brush at distance D from the grafting plane, while $U(R + \Delta R)$ is the internal energy of a *fictitious* particle with the same position of the center of mass but with slightly larger radius $R + \Delta R$ in the *same* environment of brush monomers around a nanocolloid with radius R – Fig. 8a. In all our simulations we take $\Delta R = 0.01$ so that the energy change $U(R + \Delta R) - U(R)$ is quite moderate and no overflow takes place. In addition, the efficiency of the method is substantially enhanced by computing the free energy derivative, $[F(R + \Delta R) - F(R)]/\Delta R$, for values of R which are sufficiently far apart from one another so that one can interpolate between them by an analytic function, and then use the TI method so as to get the ultimate free energy cost for insertion of a particle of arbitrary radius R at distance D from the substrate. In Fig. 8b we validate this approach by displaying the free energy derivative, $dF/dR \equiv [F(R + \Delta R) - F(R)]/\Delta R$, obtained by means of Eq. (4), to the total force, $f_{tot}(R)$, which is computed as a sum of all interactions of the nanocolloid with the surrounding monomers of the brush (i.e., an integration over the polar angle Θ in Fig. 6). From Fig. 8b it becomes evident that both methods yield results which are almost indiscernible within the statistical accuracy of the simulation. One should note, however, that the method based on Eq. (4) can be used in cases of interest where the computation of forces might be problematic.

Having thus established the method for calculating the free energy $F(R)$, we show in Fig. 9 the variation of its derivative with growing radius R for different positions D' of a repulsive nanoinclusion inside a dense polymer brush.

Eventually, in Fig. 10 we present the free energy penalty $F(z)$ for inserting a nanoinclusion of radius R at distance z from the grafting

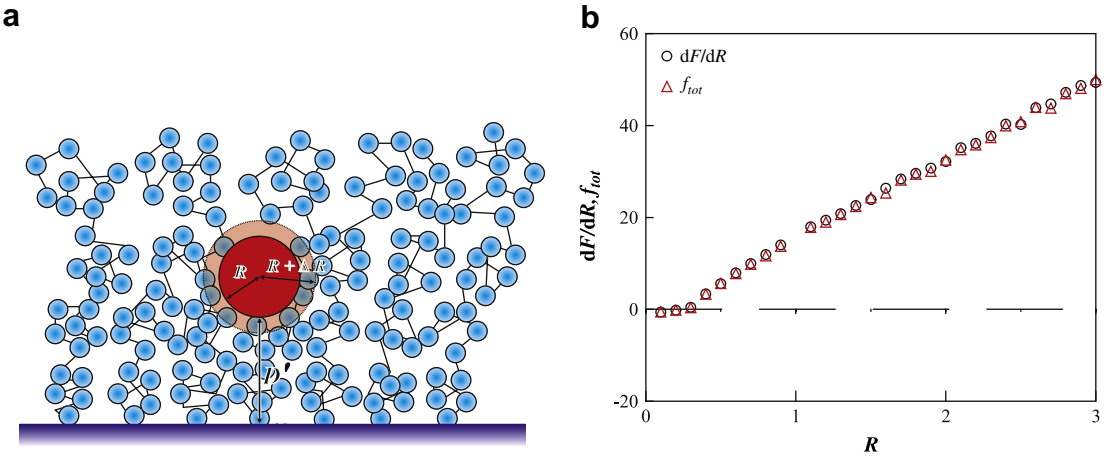

Fig. 8. (a) Schematic picture of a spherical nanoinclusion with radius R in a polymer brush. The fictitious particle has radius $R+\Delta R$. (b) Variation of the free energy derivative, $[F(R+\Delta R)-F(R)]/\Delta R$ of a spherical nanoinclusion, and of the total force, acting on it, with growing radius R. Here $N=16$, $D'=7.0$, $\Sigma=1.0$, and the nanocolloid attracts the near monomers.

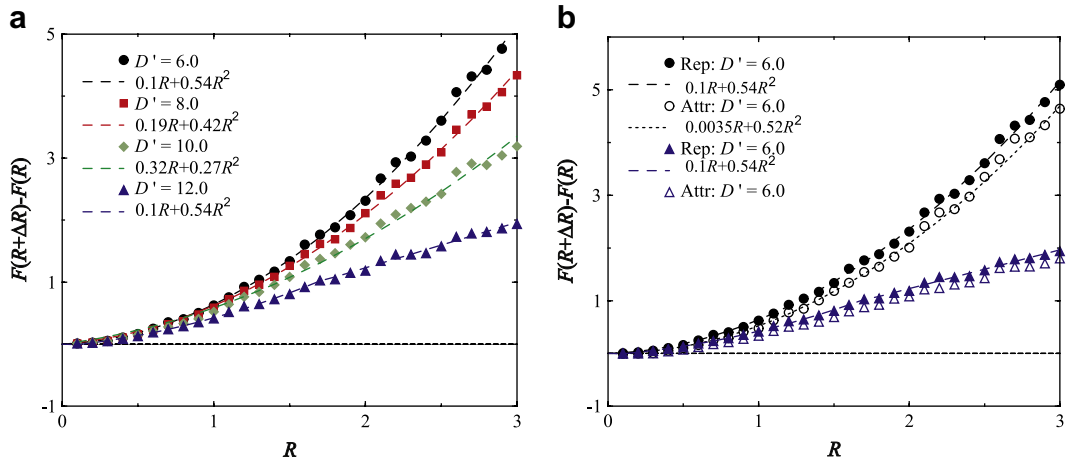

Fig. 9. (a) Variation of the free-energy derivative, $[F(R+\Delta R)-F(R)]/\Delta R$ of a spherical nanoinclusion against radius R in a polymer brush with $N=16$, $\Sigma=1.0$. The particle is softly repulsive to the monomers. Different distances from the grafting plane, D', are given as a parameter. Dashed lines denote the interpolated parabolic curves. (b) The same as in (a) but for different interaction of the nanocolloid with the brush: attraction (full symbols), repulsion (empty symbols). For $D'=6.0$ the nanocolloid is deep in the brush whereas for $D'=12.0$ (and $R\geq 1.0$) it partially shows up at the brush surface.

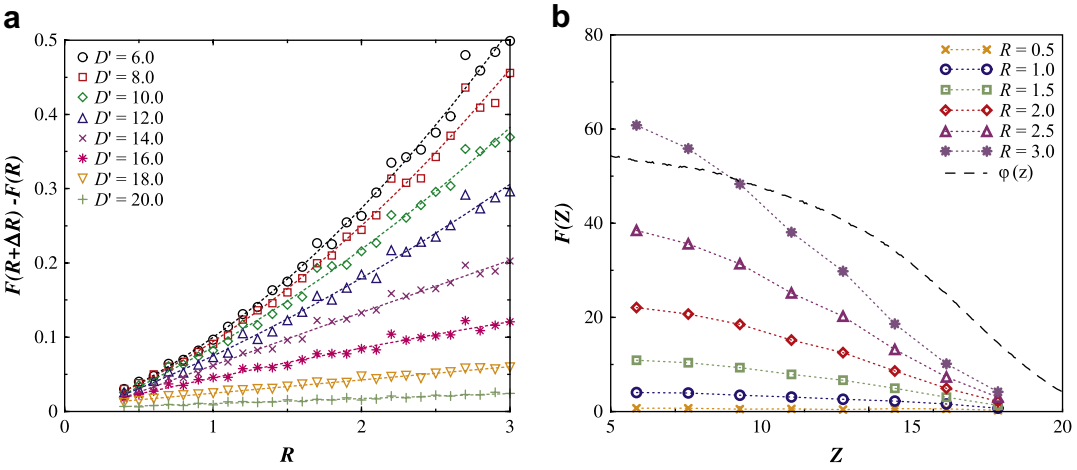

Fig. 10. (a) The same as in Fig. 9 in a semidilute polymer brush with $N=64$, $\Sigma=0.25$. Dotted lines denote interpolation curves through the data points. (b) Plot of the free energy penalty $F(Z)$ for inserting a particle into a polymer brush at distance Z from the grafting plane for several radii R. For convenience, the density profile of the monomers is also sketched (in arbitrary scaling for better visibility).

plane. Note that in this case the polymer brush is in the semidilute regime with grafting density $\Sigma = 0.25$ and longer chains ($N = 64$) were used. From Fig. 10b one can see that the monomer density $\phi(z)$ decreases significantly within the interval $6 \le z \le 20$ which explains the gradual change in the $F'(R)$ versus R relationship from parabolic (for $z \le 14$) to linear (for $z > 14$). The free energy penalty, $F(R) = \int_0^R F'(s)\mathrm{d}s$, has been calculated for arbitrary R at a distance z, using the interpolated curves from Fig. 10a. As expected, one finds an increase in the free energy cost for nanoinclusions which are placed deeper into the polymer brush whereby the cost depends strongly on the radius of the inclusion. Shallow inclusions underneath the brush surface are thus easily inserted whereas a deeper penetration is strongly hampered by the steeply rising free energy cost. Using the connection between local concentration of nanocolloidal particles $n(z)$ and $F(z)$, one can thus readily derive the concentration profiles for inclusions with arbitrary size from the variation of the free energy penalty F with z by means of the expression $\Delta F(R, z) = F(R, z) - F(R, z = \infty) = -k_B T \log[n(z)/n(\infty)]$ [36]. This expression, analog to the barometric height formula for gas particles of density $n(z)$ in an external potential $U(z)$ which role is taken here by $\Delta F(z)$, applies for a system of non-interacting particles. Since the chemical potential in such a system is constant everywhere in equilibrium, this expression accounts for the fact that the nonuniform density distribution is reflected by local changes in the excess free energy of the system. Thus the latter relationship allows the prediction of the density profile of an ideal solution of nanoinclusions at and inside a brush coating. From Fig. 10b it becomes therefore clear that these profiles diminish exponentially fast below the brush surface, and the penetration depth of larger nanoinclusions declines rapidly to zero.

5. Conclusions

In this work we suggest and validate an efficient method for calculating the excess free energy ΔF of nanoinclusions of arbitrary size, placed within polymer brushes, polymer coatings, or other cases of embedding matrix environment. The method is related to Widom's insertion test particle method [26]. As a matter of fact, it reduces to Widom's method for finding the chemical potential of particles of size r when one sets $R = 0$, $\Delta R \to r$. One of the main advantages of our method, however, is its applicability to dense environments like melts, dense polymer matrices, etc., and its easy implementation with both Monte Carlo and Molecular Dynamics simulation methods. The efficiency of the method relies on its combination with 'thermodynamic integration' whereby by sampling a few relevant sizes of an inclusion one may readily compute ΔF for arbitrary sizes. Although in this work the method has been tested and validated for spherical nanoinclusions, it can be readily used for particles of any arbitrary shape.

In the present study, relying on the afore mentioned method, we determine the excess free energy $\Delta F(R, D)$ of spherical nanocolloid particles inserted in a polymer brush. Our data analysis shows that for deep inclusions $\Delta F(R, D) \propto R^3$ whereas the free energy cost for shallow inclusions $\Delta F(R, D) \propto R^2$. We find, as expected, that the free energy penalty rises steeply as the particle is inserted deeply into the brush especially in the region of significant decline of the monomer density profile. This suggests that the concentration profiles of nanoinclusions will decrease exponentially as one goes deeper under the brush surface, especially for inclusions exceeding the monomer size by a factor of two or more. Related to this is the observation of a maximum in the buoyant force f versus distance D' relationship whereby this maximum buoyancy occurs not far beneath the brush surface. Deep inside a dense brush this buoyant force levels off due to a symmetry in the vertical distribution of monomer density around the particle. Much insight is provided also by the angular distribution of the force, exerted on the nanoinclusion by the surrounding medium which shows a significant change leading to growing buoyancy as the included particle gets closer to the brush surface.

Acknowledgments

A.M. is indebted to Prof. C. Jarzynski from the University of Maryland, USA, for his help with needed references. One of us (D.D.) received support from the Max Planck Institute of Polymer Research via MPG fellowship, another (A.M.) received partial support from the Deutsche Forschungsgemeinschaft (DFG) under project no 436BUL113/130. A.M. and D.D. appreciate support by the project "INFLUS", NMP-031980 of the VI-th FW programme of the EC.

References

[1] Fogg DE, Radzilowski LH, Blanski R, Schrock RR, Thomas EL. Macromolecules 1997;30:8433–9.
[2] Mayer ABR, Mark JE. J Polym Sci Part A Polym Chem 1997;35:3151–60.
[3] Chan VZH, Hoffman J, Lee VY, Iatrou H, Avgeropoulos A, Hadjichristidis N, et al. Science 1999;286:1716–9.
[4] Thurn-Albrecht T, Schotter J, Kästle GA, Emley N, Shibauchi T, Krusin-Elbaum L, et al. Science 2000;290:2126–9.
[5] Black CT, Murray CB, Sandstrom RL, Sung S. Science 2000;290:1131–4.
[6] Alexandre M, Dubois P. Mater Sci Eng Rep 2000;R28:1–63.
[7] Schmidt D, Shah D, Grannelis EP. Curr Opin Solid State Mater Sci 2002;6:205–12.
[8] Liu Z, Pappacena K, Cerise J, Kim J, Durning CJ, O'Shaughnessy B, et al. Nanolett 2002;2:219–24.
[9] Kim JU, O'Shaughnessy B. Phys Rev Lett 2002;89:238301–4.
[10] Lee JY, Thompson RB, Jasnow D, Balasz AC. Macromolecules 2002;35:4855–8.
[11] Thompson RB, Ginzburg VV, Matsen MW, Balasz AC. Macromolecules 2002;35:1060–71.
[12] Park C, Yoon Y, Thomas E. Polymer 2003;44:6725–60.
[13] Förster S. Top Curr Chem 2003;226:1–28.
[14] Bockstaller MR, Lapetnikov Y, Margel S, Thomas EL. J Am Chem Soc 2003;125:5276–7.
[15] Reister E, Frederickson GH. Macromolecules 2004;37:4718–30.
[16] Reister E, Frederickson Gh. J Chem Phys 2005;129:214903–13.
[17] Bockstaller MR, Mickiewicz RA, Thomas EL. Adv Mater 2005;17:1331–49. Materials.
[18] Kim JU, O'Shaughnessy B. Macromolecules 2006;39:413–25.
[19] Ballauff M, Lu Yan. Polymer 2007;48:1815–23.
[20] Milner ST. Science 1991;251:905–14.
[21] Halperin A, Tirrell M, Lodge TP. Adv Polym Sci 1991;100:31–77.
[22] Grest GS, Murat M. In: Binder K, editor. Monte Carlo and molecular dynamics simulations in polymer science. New York: Oxford University Press; 1995. p. 476–578.
[23] Grest GS. Adv Polym Sci 1999;138:149–82.
[24] Avincula RC, Brittain WJ, Carter KC, Ruehe J. Polymer brushes. Weinheim: Wiley-VCH; 2004.
[25] Dimitrov DI, Milchev A, Binder K. J Chem Phys 2007;127:084905–9.
[26] Widom B. J Chem Phys 1963;39:2808–12.
[27] Milchev A, Paul W, Binder K. J Chem Phys 1993;99:4786–98.
[28] Milchev A, Binder K. Macromol Theory Simul 1994;5:915–30.
[29] Milchev A, Binder K. Macromolecules 1996;29:343–54.
[30] Milchev A, Binder K. J Chem Phys 2001;114:8610–8.
[31] Milchev A, Binder K. J Comput Aided Mat Des 2002;9:33–74.
[32] Zwanzig R. J Chem Phys 1954;22:1420–6.
[33] Mon KK, Griffiths R. Phys Rev A 1985;31:956–9.
[34] Sokhan VP. Mol Simul 1997;19:181–204.
[35] Jarzynski C. Phys Rev E 1997;56:5018–35.
[36] Frenkel D, Smit B. Understanding molecular simulation – from algorithms to applications. San Diego: Academic Press; 2002. Section 7.2.1, p. 175.

Andrey Milchev studied Physics at the University in Sankt-Peterburg, Russia, where he got his Masters Degree in theoretical physics in 1970. In 1977 he graduated in Solid State Physics at the University of Leipzig, East Germany. Since 1979 he is in the Institute of Physical Chemistry at the Bulgarian Academy of Sciences in Sofia where now he is a full professor and head of the Group of Computer Modeling in the Department of Amorphous Materials. From 1984 to 1986 Andrey Milchev was an Alexander von Humboldt fellow at the University of Mainz, Germany, in the group of Prof. Kurt Binder, with whom a long-standing research partnership and collaboration since then exist. Andrey Milchev's interests cover computer modeling of soft condensed matter (polymers, micelles, membranes), microfluidics, diffusion and phase transitions.

Dimitar Dimitrov studied Mathematics and Informatics at the University of Plovdiv, Bulgaria, where he received his Masters Degree in 1995. In 2000, he received his PhD at the University of Food Technology, Department of Physical Chemistry, Plovdiv, Bulgaria, where he works since then. From March 1, .2006 till March 1, 2008 he was a postdoc in Prof. Binder's group at the Johannes Gutenberg University, Mainz, Germany. His research interests cover Molecular Dynamics simulations of polymeric systems, flow in micro- and nano-channels, simulations of phase transitions, etc.

Kurt Binder studied Technical Physics at the Technical University Vienna, Austria, where he got his PhD in "Technical Sciences" in 1969. He was an IBM postdoctoral fellow at IBM Zürich Research Laboratory/Switzerland in 1972–1973. In the years 1977–1983 he was a full Professor at the University of Cologne, and Director of the Institute of Theory II, Institute of Solid State Research, Research Center Jülich/Germany. Since October 1983 he is a full Professor for Theoretical Physics at the Johannes Gutenberg University in Mainz. Kurt Binder is member of numerous Scientific Councils and Academies of Sciences. Among the many awards one should mention Berni J. Alder CECAM prize (European Physical Society, 2001), Staudinger Durrer Medal (ETH Zürich, 2003) and the Boltzmann medal, 2007.